Advanced Powder Technology 25 (2014) 682–694

Contents lists available at ScienceDirect

Advanced Powder Technology

journal homepage: www.elsevier.com/locate/apt

Original Research Paper

The influence of various physico-chemical process parameters on kinetics and growth mechanism of struvite crystallisation

Eko Ariyanto [a,b], Tushar Kanti Sen [a,*], Ha Ming Ang [a]

[a] Department of Chemical Engineering, Curtin University, GPO Box U 1987, Perth, 6845 Western Australia, Australia
[b] Department of Chemical Engineering, Muhammadiyah University of Palembang, Indonesia

ARTICLE INFO

Article history:
Received 23 July 2013
Received in revised form 23 October 2013
Accepted 25 October 2013
Available online 12 November 2013

Keywords:
Struvite formation
Diffusion–reaction
Nucleation
Growth kinetics
Supersaturation

ABSTRACT

In response to struvite formation problems in wastewater treatment plants (WWTP), this mechanistic growth kinetic study of struvite crystal ($MgNH_4PO_4{\cdot}6H_2O$) was undertaken to determine the cause of preferential accumulation and to provide the remediation information to the designer of WWTP. Struvite is the mineral phase of one of the urinary tract stones of human and animals also. Here the authors presented the struvite crystal growth formation kinetics mechanism under different physico-chemical process parameters such as supersaturation ($Mg^{2+}, NH_4^+, PO_4^{3-}$), solution pH, stirrer speed, temperature, impurities and seeding conductions. To measure the growth rate of struvite crystals and to identify its various dependence system parameters, laboratory measurements were conducted in an isothermal batch 1 l stirred seeded crystalliser. Supersaturation and pH have been found to be the most influential parameters for struvite crystallisation. It was found that growth rate increased with an increase in solution pH in the pH range of 8–9. The rate of change of ortho-phosphate concentration in the bulk solution increases with increasing supersaturation ratio. The growth rate increased with increase in temperature. Higher NaCl salt concentration and higher speed also produced higher struvite growth kinetics. Fundamentally struvite crystal formation followed a classical diffusion–reaction mass transfer mechanism and overall mass transfer coefficients (K_L) under various physico-chemical process parameters have been determined. The kinetic rate constants were also calculated by fitting a first-order kinetic model and power law model to the experimental data obtained. It was also found that there was increase in product crystal size with increase in solution pH, stirrer speed and amount of salts due to slow nucleation followed by fast growth process. Struvite crystallisation may also have implication in an alternative sustainable and economical recovery of phosphorous from concentrated waste water stream.

1. Introduction

Magnesium, ammonium and phosphate are released during anaerobic digestion of solid degradation and also during sludge dewatering operation. Under certain conditions, these dissolved wastewater constituents can combine to form struvite, an orthorhombic crystalline minerals as per the following chemical reaction, where $n = 0$, 1 or 2 based on solution pH [1]

$$Mg^{2+} + NH_4^+ + H_nPO_4^{n-3} + 6H_2O \rightarrow MgNH_4PO_4 \cdot 6H_2O + nH^+ \quad (1)$$

The product of Eq. (1), i.e. magnesium ammonium phosphate hexahydrates ($MgNH_4PO_4 \cdot 6H_2O$) is commercially known as struvite. Accumulation of struvite on pipe walls and equipment surface associated with anaerobic digestion system and post-digestion processes is well known problem that plagues the wastewater treatment plant (WWTP) industry [1–5]. Remediation is often impractical and not cost effective. On the other hand, intentional and controlled precipitation of struvite is practical in the landfill and wastewater treatment plants to reduce the environmentally harmful free ammonia and phosphorous [6]. In general, struvite formation can be divided into stages: nucleation and growth. Crystal formation primarily occurs by nucleation from combination of constituent ions called embryos and nuclei growth in sequence, i.e. enlargement of crystal until equilibrium [7–10]. Predicting and controlling struvite nucleation and growth is fundamental to crystalliser design. Therefore, predicting struvite formation potential is not only critical to struvite problem but also for remediating existing struvite damage. However, predicting or controlling these stages are complex as it is controlled by a combination of thermodynamic and mass transfer properties along with various physico-chemical factors, such as solution pH, supersaturation, mixing, crystal sizes and the presence of foreign impurities. The struvite crystallisation process, like all other crystallisation process is thermodynamically

* Corresponding author. Tel.: +61 8 92669052.
E-mail address: t.sen@curtin.edu.au (T.K. Sen).

0921-8831/$ - see front matter © 2013 The Society of Powder Technology Japan. Published by Elsevier B.V. and The Society of Powder Technology Japan. All rights reserved.
http://dx.doi.org/10.1016/j.apt.2013.10.014

unstable and well proceed towards a stable state through nucleation and crystal growth [11].

In our previous work [12], a lab scale investigation of spontaneous nucleation mechanism of struvite formation was reported which is the first phase of struvite crystalliser. It was found that the time taken for nucleation to occur (often indicated by the induction time) is a measure of struvite nucleation and it was decreased with an increase in solution pH, temperature and degree of supersaturation. Overall induction time is primarily controlled by the reaction limited homogenous and heterogeneous nucleation process. Overall precipitation kinetics can be separated into two phases; nucleation and growth. After the induction time, crystal growth continues until equilibrium is reached [11] and therefore growth is the second part of crystallisation kinetic which occurs when clusters aggregate themselves or diffuse onto the surface of diffusive bodies [7–10]. Crystal growth also depends on various physico-chemical process parameters such as solution pH, degree of supersaturation, mixing, crystal size, temperature, and presence of impurities [8,9]. All these physico-chemical process parameters also depend on wastewater effluent's origin and treatment technology. Hence this study was undertaken to identity the struvite crystal growth mechanism kinetics and to provide a new growth kinetic data set under various process conditions.

Supersaturation and pH have been reported to be the most influential parameters for struvite crystallisation [11]. Struvite is highly soluble at acidic pH and highly insoluble in alkaline pH [2]. Thus its precipitation can be controlled by pH adjustment as well as by alternation of supersaturation. Struvite formation through Eq. (1) will be favoured to precipitate if the ion activity product (IAP) of Mg^{2+}, NH_4^+, and PO_4^{3-} is greater than its solubility product (K_{SP}). The *IAP* is controlled by solution pH. The both NH_4^+ and PO_4^{3-} ion activities are pH dependent [13]. Higher percentage of P-removal through struvite formation with increase in solution pH was reported by various investigators [4,14–17]. Nelson et al. [18] studied the effect of pH on struvite precipitation on an anaerobic swine lagoon wastewater system. They have reported that the rate of removal of phosphorous concentration was increased with increase in pH from 8.4 to 9.0 and followed first order kinetics.

Although temperature has a lower impact on struvite precipitation compared to other system parameters, such as pH and supersaturation [19], it influenced solubility of struvite. The experiment conducted by Aage et al. [20] and Burns and Finlayson [21] showed the solubility of struvite increased with increase in temperature. However, Bhuiyan et al. [22] reported that the solubility of struvite increased with temperature, until 35 °C, and then it is decreased. An increase in temperature strongly influences the growth rate and the efficiency of the phosphate removal through struvite crystallisation [23].

A large number of studies on struvite crystallisation is limited on the application oriented thermodynamics such as struvite solubility and much less on the kinetics [2]. The crystal growth kinetics is also greatly influenced by hydrodynamic condition. In industrial practice, there is always a stirrer or other device in places that not only ensure homogeneity between crystals and solution but also accelerates the growth of crystals. Uludag-Demirer and Othman [24] reported that there was no significant effect of stirring on struvite precipitation. Investigation conducted by Kim et al. [25] shows that high mixing intensity (u) and mixing duration (t_d) at above 2×10^5 was effective for the removal of nitrogen and phosphorous. This indicated that the effect of mixing was not only accelerate nucleation process but also effective in the removal of nitrogen and phosphorus through struvite formation. Stirrer speed can create segregation and attrition which affect the spontaneous nucleation rate, resulting in a change in crystals number, size, and morphology [7,26]. Although there are few reported results on stirrer speed effect, the interrelationship between hydrodynamics and crystallisation is complex and poorly understood and, hence, a better understanding of the effect of hydrodynamic condition on crystallisation processes is of significant industrial importance and therefore this study was also undertaken.

Presence of impurities in WWTP effluent (e.g., Cl^-, K^+, etc.) may influence the supersaturation of struvite by reacting with its component ions, Mg^{2+}, PO_4^{3-}, and NH_4^+ in solution. Further, the presence of impurities in solution can block or inhibit struvite crystals formation. The presence of impurities may also increase or decrease the crystal size [7]. The presence of calcium and carbonates impurities in solution affected the struvite growth rate [1]. Kabdasli et al. [27] reported that the presence of sodium, calcium, sulphate and carbonate ions affected the induction time, struvite crystal morphology, and sizes. Therefore knowledge of the effect of solution pH, temperature, impurities, seed and hydrodynamic condition on the struvite crystallisation fundamentals is very much important for struvite formation. Several mechanisms including surface energy theory, adsorption layer theory and transport limitation model based on diffusion reaction theory have been proposed to explain crystal growth [4,11]. The relative influence of each mechanistic model can change over time due to changes in physico-chemical process parameters such as supersaturation, solution pH, temperature and crystal size. Therefore, this study was attempted to explore the effect of solution pH, supersaturation, impurities, crystal size and hydrodynamic condition on the struvite crystallisation mechanism especially on the kinetics of struvite crystal growth and to determine the quantitative importance of transport and surface integration struvite formation model. This mechanistic growth kinetics study is essential for the design and optimisation of struvite crystallisation process. Various kinetic parameters including activation energy, diffusivity and mass transfer coefficient for struvite crystal growth under various process conditions have been reported here which is new compared to the existing reported results. Further, this study was taken first time to synthesise single-phase struvite crystals by mixing solutions of $MgCl_2{\cdot}6H_2O$ and $NH_4H_2PO_4$ at room temperature. Struvite precipitation kinetics was studied under different condition to find out the kinetic rate constant and a diffusion–reaction growth mechanism has been established here.

2. Materials and methods

2.1. Chemicals

Struvite precipitation reaction was carried out by using magnesium chloride hexahydrate ($MgCl_2{\cdot}6H_2O$), and dihydrogen ammonium phosphate ($NH_4H_2PO_4$). Stock solution of $MgCl_2{\cdot}6H_2O$, as Mg^{2+} provider, is made by dissolving crystals of $MgCl_2$ in distilled water. The stock solution of $NH_4H_2PO_4$, as NH_4^+ and $H_2PO_4^-$ provider, are prepared in the same manner. Both solutions were stored separately and only mixed just prior to any experimental run. Extreme care was taken to keep the solution from dust, insoluble matter, etc. In addition, all solutions were filtered before experimental use. The solution pH was adjusted using 0.1 M sodium hydroxide (NaOH) solution.

2.2. Experimental set-up and procedure

The experimental setup is shown schematically in Fig. 1. All experiments were performed in the laboratory-scale jacketed stirred batch crystalliser with a working volume of 1 l. The crystalliser consists of a cylindrical glass vessel with a round bottom and 130 mm internal diameter. The vessel was fitted with four vertical equidistant glass baffles (15 mm × 83 mm) which were placed along with the wall of the crystalliser. The solution was stirred

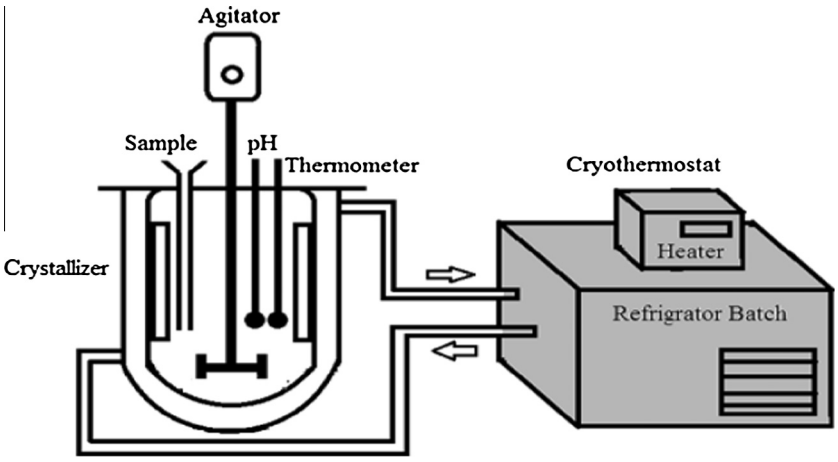

Fig. 1. Experimental setup of a batch crystalliser.

by a stainless steel impeller (number of blades 4; blade length 20 mm; blade width 20 mm) with the smoothest surfaces to reduce the resistance that could trigger a nucleation of struvite crystals. The impeller was located at one-third of the working liquid level from the crystalliser bottom. The crystalliser was covered with a steel plate to minimise evaporation of solution. Temperature control within the crystalliser was achieved by pumping water from water batch enclosed in a cryothermostat with PID regulator for temperature control through the water jacket.

The study was conducted in same batch crystalliser with pH control at 25 °C. One litre of supersaturated solution was introduced into the crystalliser. After the supersaturated solution reached the desired temperature and pH, the supersaturated solution was allowed to settle at constant temperature and pH and no visible turbidity was observed for 20 min. Seed crystals of struvite were added into the crystalliser containing supersaturated solution at 25 °C. The pH was adjusted by addition of NaOH solution. The pH metre was standardised with pH 4, 7 and 10 buffer solutions. The experiment was conducted for 120 min with 1, 5, 10, 15, 20, 30, 40, 60, 80 and 120 min sampling times. An amount of 2 ml solution was withdrawn at each sampling time from the crystalliser by a syringe and filtered through a 0.22 μm filter medium. The product struvite crystal was filtered and oven dried overnight at 35 °C and used for crystal size, weight, FTIR and XRD analysis. The filtered product samples were then analysed for magnesium, ammonia, and ortho-phosphates. Orto-phospahte and ammonia concentration were measured by UV–spectrophotometer. Magnesium analysis was performed by atomic absorption spectrophotometer. The crystal size distributions were measured by laser diffraction with a Malvern Master Sizer 2000. The detailed operating conditions are listed in Table 1 for each experimental run.

Investigation of stirrer effect was carried out at temperature 25 °C and at pH 8. The stirrer speed was varied from 50 to 120 rpm. The stirrer speed was selected to ensure that seed crystals introduced would be well suspended in the crystalliser. Experiments were also conducted by suspending the seed crystals in a saturated solution to ensure that no attrition occurred to the seed crystals under all selected stirrer speed used for this study. The saturated solution was prepared by dissolving struvite crystal for 24 h.

2.3. Seed preparation

Seeds were prepared by dissolving synthetic crystals of specific amount in a supersaturated solution and agitated gently in order to get the agglomerate. Crystals that have been separated from agglomerate crystals was taken using a plastic pipette and kept into a petri disk. Crystals were then dried to reduce the water content at room temperature. The dried crystals were transferred into a small container and the crystals were rinsed with two drop of deionised water, and dried immediately with the filter paper. Seed crystal size was determined by Malvern Master Sizer 2000 and morphology was measured by scanning electron microscope. The Fourier transform infrared spectroscopy (FTIR) was used to analyse potential changes in the inner structure of struvite crystals. These dried seed crystals were used to crystal growth experiments.

2.4. Crystal growth calculation

Crystal growth calculation was done through the use of crystal size distribution plots as shown in Fig. 2. This curve represents the dependence between the number of crystal per unit volume and crystal size. It is assumed that, in a suspension of growing crystals (seed crystal), at time t, the crystal size is L_1. After a certain time, the seed crystal grown in supersaturated solution with size of L_2. The seed crystals with the original size L_1 have grown to size, ΔL. Therefore, the average growth rates of crystals are

$$G(L,t) \cong \frac{L_2 - L_1}{(t+\Delta t) - t} = \frac{\Delta L}{\Delta t} \tag{2}$$

where Δt is the time needed for constituent ion of struvite to reach equilibrium.

2.5. Supersaturation calculation

The supersaturation was calculated using the specification PhreeqC program [12,28]. PhreeqC is a computer program designed base on an ion-association aqueous and saturation-index (SI) calculation [28].

$$\mathrm{SI} = \log S = \log \frac{[Mg^{2+}][NH_4^+][PO_4^{3-}]}{\frac{K_{sp}}{\gamma_{Mg^{2+}} \cdot \gamma_{NH_4^+} \cdot \gamma_{PO_4^{3-}}}} \tag{3}$$

From Eq. (3) the relative supersaturation is given by

$$S = \frac{[Mg^{2+}][NH_4^+][PO_4^{3-}]}{\frac{K_{sp}}{\gamma_{Mg^{2+}} \cdot \gamma_{NH_4^+} \cdot \gamma_{PO_4^{3-}}}} \tag{4}$$

The thermodynamic solubility product of struvite on equilibrium with pure and solid phase struvite is as follows [22];

Table 1
Various crystallisation experimental conditions.

No.	Temp (°C)	pH	Supersaturation	Stirring speed (rpm)	Seed size (μm)	Seed loading (mg)	Impurity (ppm)
1. (Fig. 5)	25	8	2.04	120	24.3	100	0
2. (Fig. 6)	25	8.5	2.04	120	24.3 43.5 84.8	40	0
3. (Figs. 7 and 8)	25	8	2.2 3.2 6.0 10.0	120	24.3	40	0
4. (Figs. 9–12)	25	8.0 8.5 9.0	2.04	120	43.5	100	0
5. (Fig. 13	25	9.0	Saturated solution	120 100 50	43.5	100	0
6. (Figs. 14 and 15)	25	9.0	2.04	120 100 50	43.5	100	0
7. (Fig. 16)	20 25 30	9.0	2.04	120	43.5	100	0
8. (Fig. 17)	25	8.0 8.5 9.0	1.95–10.23	120	43.5	100	0
9. (Fig. 19)	25	8.5	2.04	120	43.5	100	0 50 100 200

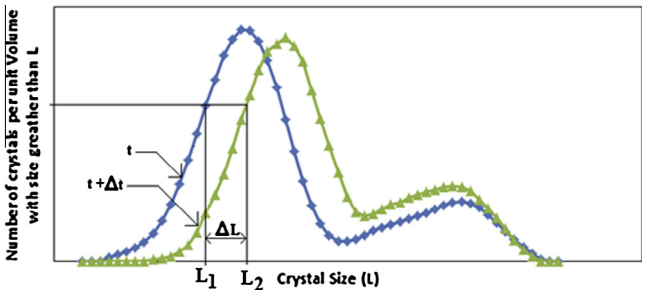

Fig. 2. Determination of growth rate from cumulative size distribution.

$$K_{sp} = \gamma_{Mg^{2+}}[Mg^{2+}] \cdot \gamma_{NH_4^+}[NH_4^+] \cdot \gamma_{PO_4^{3-}}[PO_4^{3-}] \quad (5)$$

where K_{sp} is solubility product in terms of ion activity and γ_i is activity coefficient of the ion i.

2.6. Kinetic study and theory

In order to investigate the mechanism of crystallisation, the crystal growth process was analysed using first and second-order kinetic models. The first-order kinetic model was applied to the experimental results as per method by Nelson et al. [18], Quintana et al. [29] and Rahaman et al. [30]. This model can be written simply as follows;

$$-dC/dt = k(C_t - C_S)^n \quad (6)$$

where k is rate constant, n is order of reaction, C_t is the reactant concentration at time t, C_S is the reactant concentration at solubility and $-dC/dt$ is the rate of reactant phosphate disappearance.

The linearised form of first-order kinetic model of Eq. (6) can be written as.

$$\ln(C_t - C_S) = -k_1 t + \ln(C_i - C_S) \quad (7)$$

where C_t is the reactant concentration at time t, C_i is initial reactant concentration, t is reaction time and k_1 is first-order rate constant. Eq. (7) can also be written as

$$\ln\left(\frac{C_t}{C_S} - 1\right) = -k_1 t + \ln\left(\frac{C_i}{C_S} - 1\right) \quad (8)$$

where $C_t/C_S = S_t$ and $C_i/C_S = S_i$.Therefore Eq. (8) can be further rewritten as

$$\ln(S_t - 1) = -k_1 t + \ln(S_i - 1) \quad (9)$$

where S_t is supersaturation at time t and S_i is supersaturation at time $t = 0$. A plot of $\ln(S_t - 1)$ against time should give a straight line with a slope $-k_1$.

Similarly, the linearised form of a second-order kinetic model can be written as

$$\frac{1}{(C_t - C_S)} = \frac{1}{(C_i - C_S)} + k_2 t \quad (10)$$

Or

$$\frac{1}{(S_t - 1)} = \frac{1}{(S_i - 1)} + k_2 C_S t \quad (11)$$

where k_2 is second-order rate constant. A plot of $1/(S_t - 1)$ against time should give a straight line with slope of $-k_2$.

3. Results and discussions

3.1. Struvite crystal product characteristics

Scanning electron microscope with EDS analysis at seed and struvite product crystals at a solution pH of 9 and temperature 25 °C are shown in Fig. 3(a) and (b), respectively. The product crystals have a similar shape (Fig. 3(b)) to the seed crystals (Fig. 3(a)) indicating there was no phase transformation during growth. Further struvite crystals have a distinctive orthorhombic structure along with cubic and needle like structures shown in Fig. 3(a) and (b). Similar, struvite crystals shape have been reported in our earlier work [12].

According to EDS analysis, the phosphorus atomic concentration is equal to magnesium concentration. Fig. 3(a) shows that the seed struvite crystals formed as no trace of other compounds

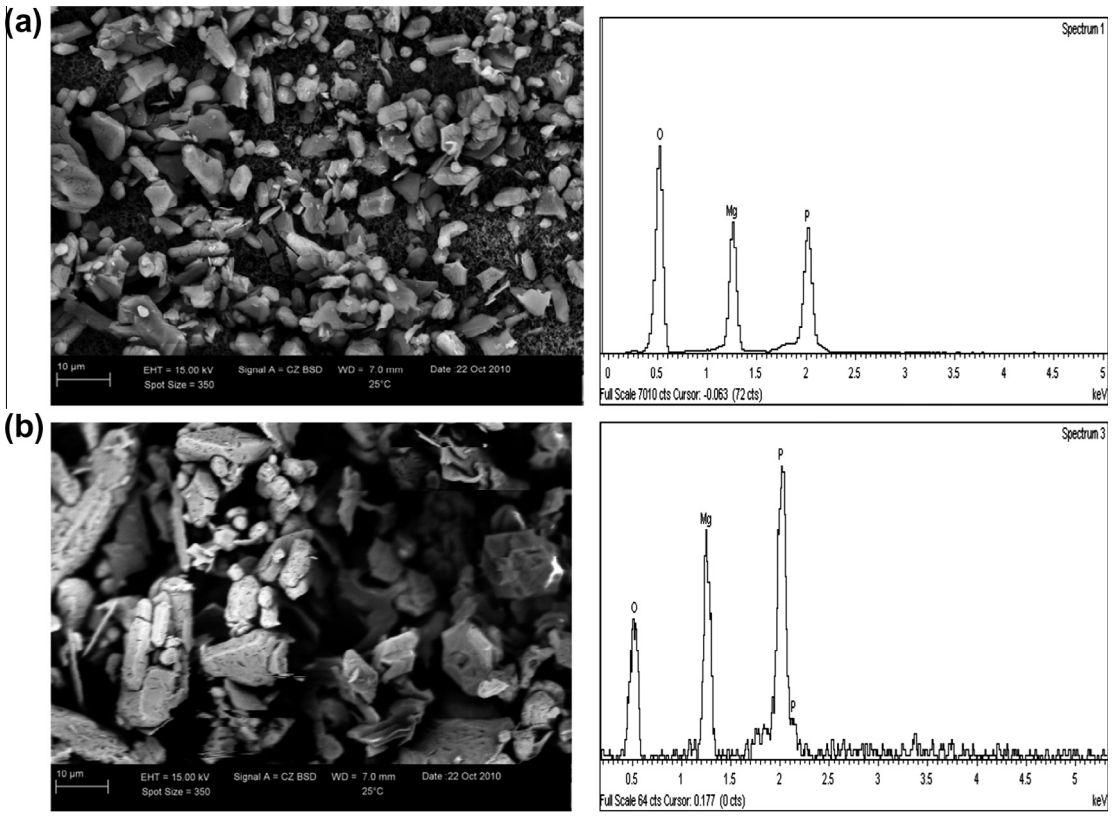

Fig. 3. SEM of struvite; (a) Seed crystals; (b) product crystal.

have been found. The EDS of product struvite crystals analysis matches with seed struvite crystals. It also showed a composition of P, Mg and O. Struvite product when crystallisation was occurred at pH 9 shows that phosphorus peak was higher than magnesium peak. The formation of this precipitate at the surface of crystals would thus explain the multitude of background peak observed on FTIR pattern while struvite peak are identified.

The Fourier transform infrared spectroscopy (FTIR) was used to analyse potential changes in the inner structure of struvite crystals. Fig. 4 shows the FT-IR spectrum of struvite seed and product struvite crystal. The absorptions occurring at 3421, 3424.5 cm^{-1} are due to O–H and N–H stretching vibration. This also suggests the presence of water of hydration. The absorption occurring at around 2921 and 2914.5 cm^{-1} is due to NH_4^+ ion [31]. The weak bands appeared at 2341 cm^{-1} in the spectrum can be assigned due to H–O–H stretching vibrations of cluster of water molecules of crystallisation. The absorption occurring around 1472.5 and 1434 cm^{-1} have been attributed to N–H bending vibration [32]. The absorptions taking place at around 1057.5 and 975.5 cm^{-1} are due to ionic phosphate [33]. A medium absorption band at around 771 and 778 cm^{-1} indicates the wagging modes of vibration of the coordinated water and the Metal–Oxygen bond in the complex.

According to FTIR spectra patterns, as shown in Fig. 4(a) and (b), it was confirmed that no substantial crystalline change was found between seed crystals and crystal product. However, the minor differences in the relative intensities of their peaks might be attributed to differences in the degree of crystallinity of the samples. Details FTIR and SEM characteristics of product struvite crystals under various solution pH, temperature, stirrer speed, supersaturation are presented elsewhere [34]. We are also investigated CSD

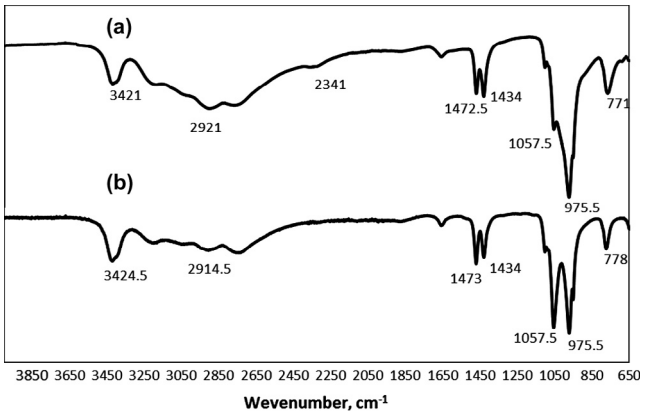

Fig. 4. FTIR spectra of struvite crystals. (a) Seed crystals; (b) product crystal.

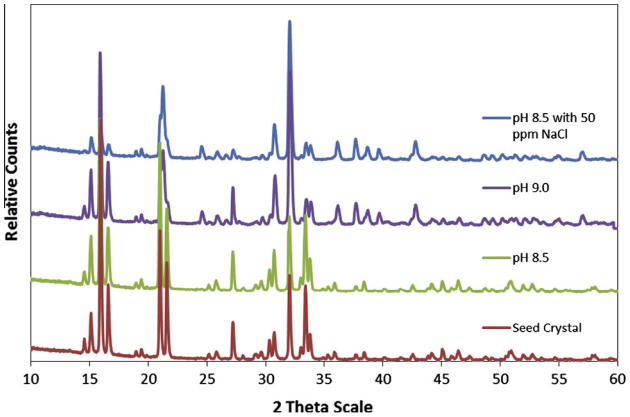

Fig. 5. XRD trace for seed crystals and struvite product at different solution pH.

product crystals under various process conditions by Malvern Master Sizer 2000 for which plots are not presented here.

Fig. 5 showed the XRD analysis of seed and product struvite crystal. XRD data indicated single-phase struvite (orthorhombic) space group with the experimental lattice parameters of $a = 11.215$, $b = 6.954$, $c = 6.141$. In Fig. 5, the patterns confirmed that orthorhombic struvite was dominant crystal phase and no difference in the XRD pattern observed for seed crystals and product crystal. Similar observations were also reported by many investigators [11,35,36].

3.2. Effect of seed loading and size on crystal growth

The effect of seed loading on the decay of supersaturation in solution is shown in Fig. 6. Decay of supersaturation give indication of struvite formation. It can be seen from the plot that the increasing seed loading increased rate of struvite formations. Increasing mass seeds can provide the more available surface area for crystal growth, more solute molecules can be precipitated on these surfaces, enhancing the growth rate and thus weakening the nucleation rate accordingly. However, in the case of lower seed loading, the contribution of newly generated secondary nuclei to the decay of supersaturation becomes significant [37,38].

Results of decay of relative supersaturation measurement versus time for struvite on different size of seed crystals are presented in Fig. 7. From Fig. 7 the growth rate increases with decrease in seed size. The increased rate of crystal growth was caused by increase in total area available for growth in which the smaller seed crystals providing a larger surface area compared to larger seed crystals of the same mass [37].

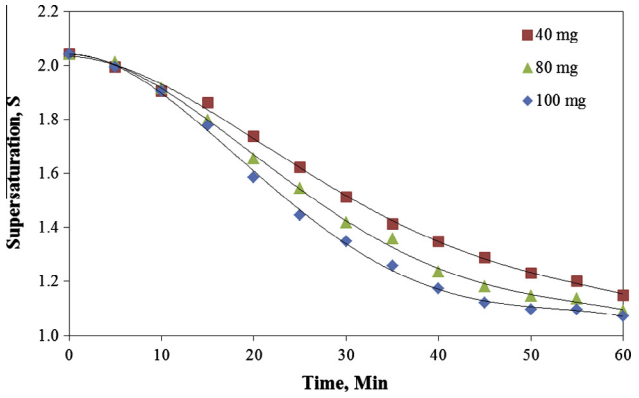

Fig. 6. Effect of seed loading on the decay of relative supersaturation. Solution pH = 8; temp = 25 °C; seed loading = 100 mg; seed crystal size = 24.3 μm; agitation speed = 120 rpm.

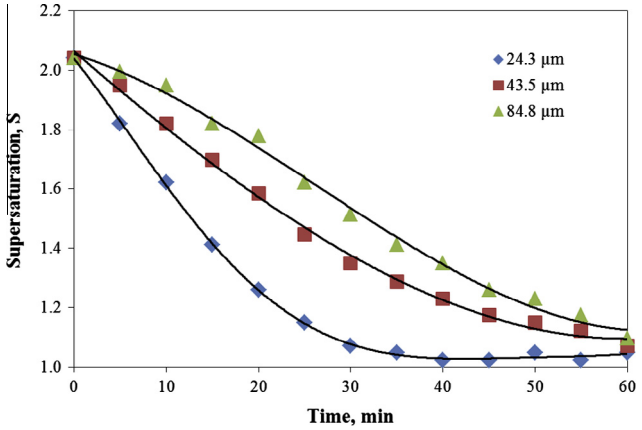

Fig. 7. Effect of average seed size on the decay of relative supersaturation. Solution pH = 8; Temp = 25 °C; Seed loading = 100 mg; agitation speed 120 rpm.

3.3. Effect of solution pH and supersaturation on struvite crystal growth kinetic

Solution pH is one of the important factors for the removal of nutrient such as nitrogen and phosphorus from solution [16,39] by struvite precipitation. A small variation of solution pH may reduce available surface area to the growth unit caused by changes significantly in the zeta potential of the particle leading to the eventual destabilisation of suspension by aggregation [35]. Controlling solution pH during struvite crystallisation not only could increase struvite formation [39] but also could accelerate growth rate [40].

To investigate the effect of supersaturation on the formation of struvite, the disappearance of ortho-phosphate ions were monitored during the experimental run. As shown in Fig. 8, the percentage removal of PO_4 was increased with increase in supersaturation at a constant solution pH of 8 and it is more significant at higher supersaturation.

Fig. 8 also shows different results obtained for the percentage PO_4 removal at constant pH experiments. The percentage of PO_4 removal was always higher at higher supersaturations.

In our earlier reported studies, the change of solution pH was an indicator of struvite nucleation [12]. As struvite precipitates, it triggers a release of proton ions in solution and hence a change in pH occurs during the nucleation process. The drop in pH is characteristics of the speed at which the first crystals of struvite occurs and is linked to the rate of struvite formation. Fig. 9 showed the change in solution pH with time for range of supersaturation of 2.2–10. It was found that the increase in supersaturation leads to an increase in the change of solution pH and a reduction in induction time (Fig. 9).

From this experiment, the PO_4 concentration of 2 mMol/L (189.9 mg/L) was chosen for conducting experiments on the effect of solution pH on PO_4 removal by struvite precipitation (Fig. 10). The decay of supersaturation of PO_4 concentration in bulk solution reached steady state after 30, 40, and 60 min with the addition of seed crystal at a solution pH of 8.0, 8.5 and 9.0 respectively. For solution pH 8, 12.6% of PO_4 was removed from the solution. Percentage removal of PO_4 increased significantly with higher solution pH. Increasing solution pH from 8 to 9 increased PO_4 removal to 58.9%. It can be seen that operating the crystalliser at pH 9.0

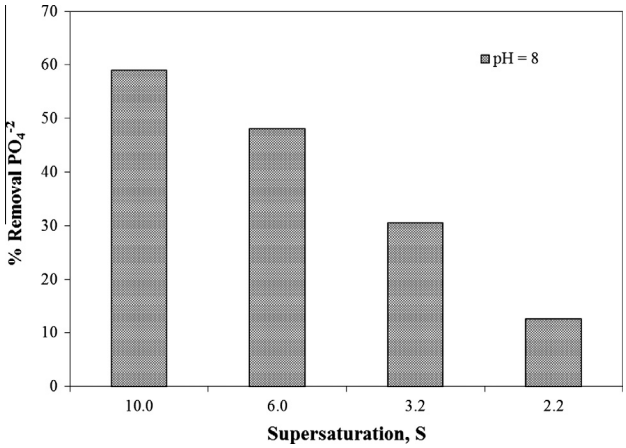

Fig. 8. Effect of supersaturation on the removal of PO_4. Solution pH = 8; temp = 25 °C; seed loading = 40 mg; seed crystal size = 24.3 μm; agitation speed = 120 rpm.

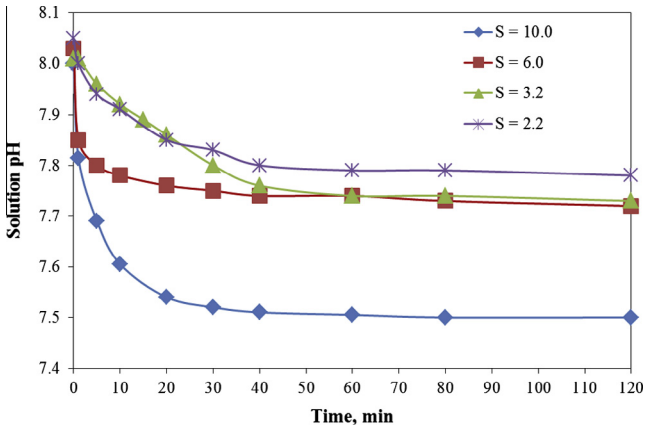

Fig. 9. Change of solution pH with time at various supersaturations. Solution pH = 8; temp = 25 °C; seed loading = 40 mg; seed crystal size = 24.3 μm; agitation speed = 120 rpm.

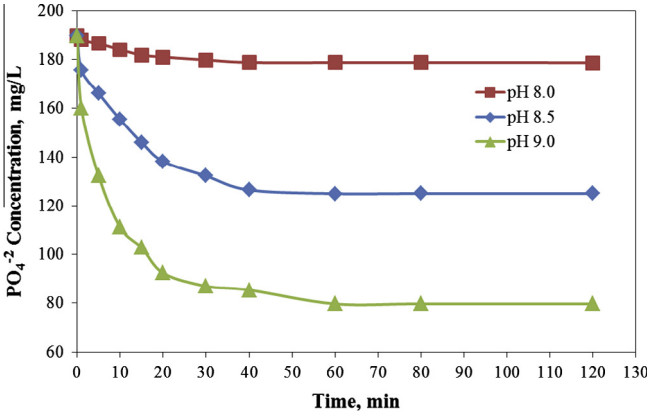

Fig. 10. Effect of solution pH on PO_4^{2-} removal. Temp = 25 °C; seed loading = 100 mg; seed crystal size = 43.5 μm; agitation speed = 120 rpm.

becomes imperative for higher PO_4 removal [41]. On the other hand, the low pH may be an option to prevent scale formation of struvite crystals in wastewater treatment plant (WWTP).

From Fig. 11, it was found that the higher PO_4 removal efficiency occurred at higher solution pH with faster rate. The kinetic experimental data were fitted by plotting ln (C–C_e) versus *time* (t) which gives a straight line with different slopes which are shown in Fig. 11a–c, respectively. The values of linear regression coefficients (R^2) indicate the applicability of first-order kinetic model to the experimental observation. The fitted rate constants (k_1) were 3.7, 5.1 and 6.9 h^{-1} for solution pH of 8.0, 8.5 and 9.0, respectively. The obtained rate constant is very much comparative with the others reported results [18,29,30]. The results indicate that the increasing solution pH increases the rate of struvite precipitation. However, the increasing rate of precipitation was indicated by increasing supersaturation due to change in solution pH. Based on the calculation by using PhreeqC model, the changing solution pH increased supersaturation from 1.23 to 10.23. This investigation was extended to identify the various rate constant of struvite precipitation at different solution pH. The supersaturation was selected at a value of 2.04 which is close to solubility of struvite crystals. So, rate of struvite precipitation is slow and easily identify its secondary nucleation. Based on PhreeqC model calculation, the concentration of Mg, PO_4 and NH_4 conducted in batch crystalliser was 1.05 mMol/L, 1.63 mMol/L and 2.63 mMol/L for a solution pH 9.0, 8.5 and 8.0, respectively. The supersaturation was monitored during the experimental run by monitoring concentration of Mg, PO_4 and NH_4 over the period of time. The PhreeqC model was used to calculate decreasing supersaturation. The results are presented in Fig. 12.

The effect of solution pH on the decay of supersaturation in solution is shown in Fig. 12. It was observed from Fig. 12 that with the increasing solution pH, the relative supersaturation decreases more quickly. This is because of increase in phosphate ions concentration with the increase in solution pH, while the higher pH values, solute in solution accelerates to deposit on the crystal surface, and hence the growth rate. The marked dependence of growth rate on pH values is probably due to the change of surface charge on crystal surface [42,43]. Similar observations were also reported by Rahaman et al. [30] for different system.

Subsequently the experimental data were fitted with both first-order (Eq. (9)) and second-order kinetics model (Eq. (11)) which are presented in Fig. 13(a) and (b), respectively. The higher value of linear regression coefficient (R^2) showed that the decay of relative supersaturation followed first order kinetics which also confirms the high dependence of growth observed at higher stirrer speeds. The fitted rate constants (k_1) for first-order kinetic model were 3.0, 4.3 and 5.8 h^{-1} for a solution pH of 8.0, 8.5 and 9.0, respectively. Similar trend was observed by Nelson et al. [18].

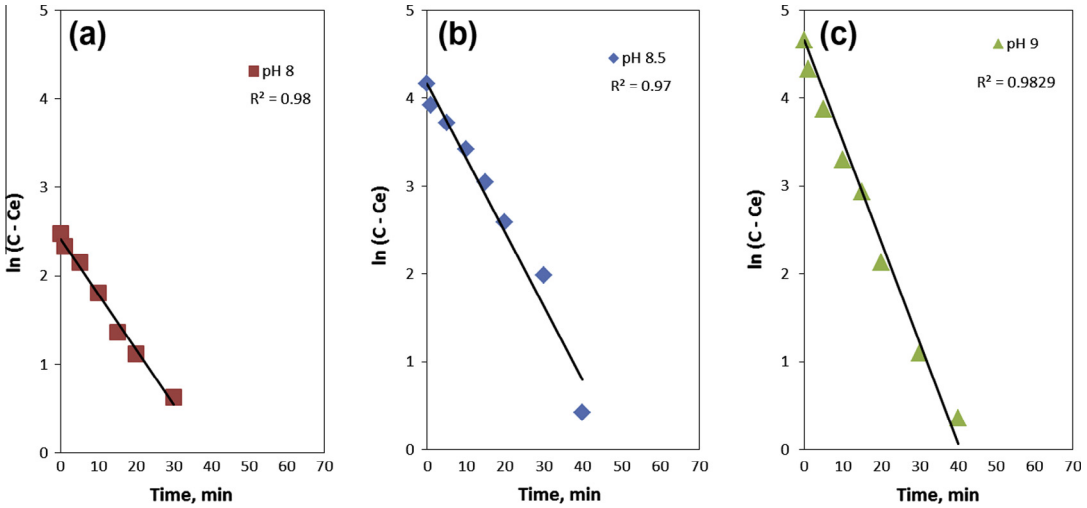

Fig. 11. Plot of ln (C–C_e) versus time at various solution pH. Temp = 25 °C; seed loading = 100 mg, seed size = 43.5 μm; agitation speed = 120.

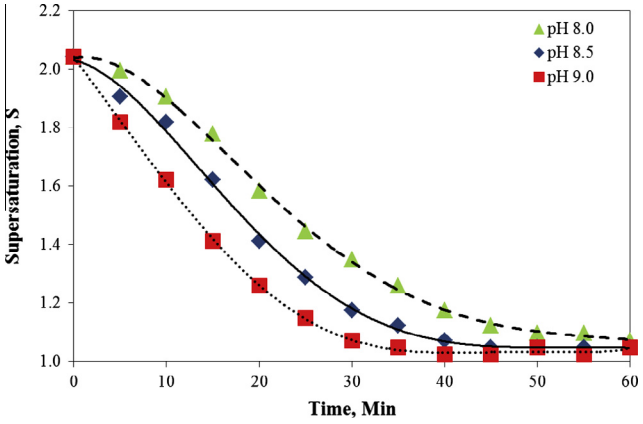

Fig. 12. Effect of pH on the decay of supersaturation curve. Temp = 25 °C; supersaturation = 2.04; seed loading = 100 mg; seed size = 43.5 μm; agitation speed = 120 rpm.

The obtained first order rate constant from this study was 5.8 h^{-1} at a solution pH of 9.0 which comparatively lower value with 12.3 h^{-1} reported by Nelson et al. [18]. This lower value in rate constant is advantageous for crystalliser design. The lower rate constant reported in the present study is most likely a result of different supersaturation in the measurement and hence different concentration driving force.

3.4. Effect of stirrer speed

The range of stirrer speeds was selected to ensure homogeneous suspension. Further no significant breakage of the crystals taken place at three stirrer speeds. Seed sizes were suspended in a saturated solution at the various stirrer speeds for 15 min before analysing the resultant crystals for their size distribution (Fig. 14). Fig. 14 clearly shows that crystal size distribution for seed crystals and stirrer speed were not significantly changed. Thus the selected stirrer speeds were in the range 50–120 rpm.

In this study, the solution supersaturation was calculated by adjusting the concentration of Mg, PO_4 and NH_4 at constant pH. The solutions of Mg:NH_4:PO_4 were made in a theoretical equimolar ratio of 1:1:1. To investigate the effect of stirrer speed on the formation of struvite, the supersaturation was monitored during the

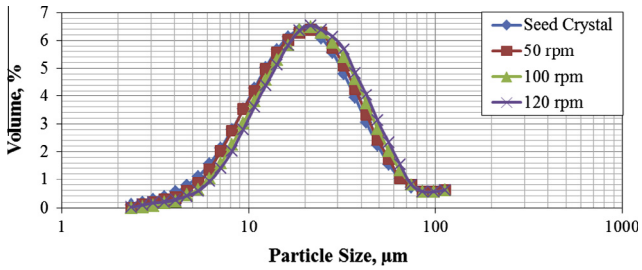

Fig. 14. Crystal size distribution versus stirrer speeds for 15 min. Solution pH = 9; Temp = 25 °C; seed loading = 100 mg; seed size = 43.5 μm.

experimental run by examined concentration of Mg, PO_4 and NH_4 species. The decay of relative supersaturation during precipitation is shown in Fig. 15. The decay of relative supersaturation curves for different stirrer speeds showed that decay of relative supersaturation is a strong function of the stirrer speed. It can be observed that the induction period is significantly affected by stirrer speed. The decay of relative supersaturation curves showed that the induction time of secondary nucleation at low stirrer speed of 50 rpm was 10 min but dropped to about 1 min when 100 and 120 rpm. This shorter induction time indicated higher rates of secondary nucleation at higher stirrer speeds. Higher speeds caused higher fluid and seeds velocities, increased the frequency of crystal-crystal, crystal-impeller, and crystal-crystalliser surface collisions, thereby causing higher rates of secondary nucleation as reported by Frawley et al. [37]. Moreover, higher rate of secondary nucleation was also may be induced by fluid shear nucleation. Fluid shear nucleation means that when a crystal moves in liquid at higher speed, nuclei sweep away from the surface.

After the induction time, crystal growth continued until equilibrium is reached. The equilibrium time of struvite precipitation was observed by decreasing supersaturation in bulk solution. For the three stirrer speeds of 50, 100, and 120 rpm, the equilibrium time were 60, 45, and 40 min, respectively. Fig. 15 also showed that more growth occurred at higher stirrer speeds as the equilibrium solution concentration was much lower at higher stirrer speed.

The experimental data were fitted with both first-order (Eq. (9)) and second-order kinetics (Eq. (11)) model equation and these are shown in Fig. 16(a) and (b), respectively. The value of linear regression coefficient (R^2) resulting from Fig. 15a showed that the decay of supersaturation supersaturation followed first order kinetic

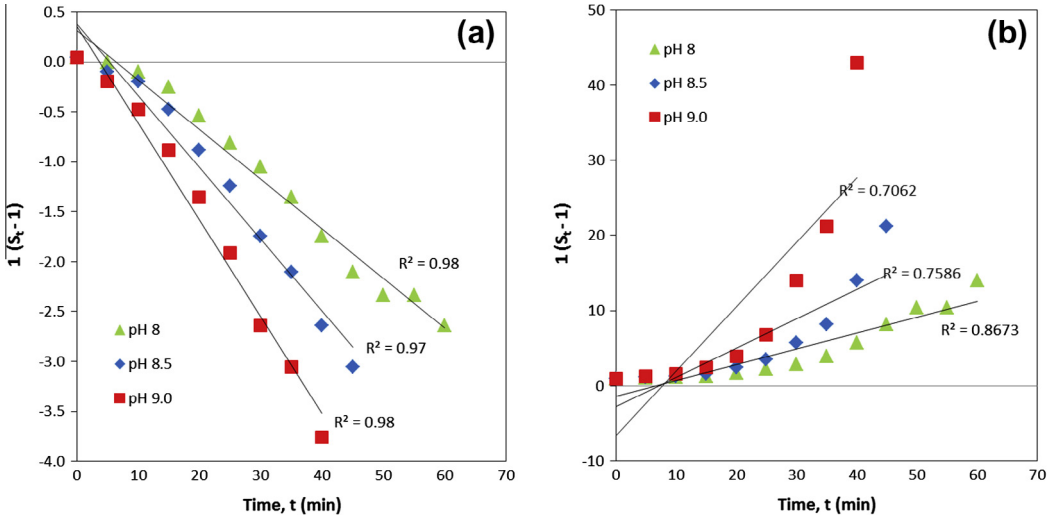

Fig. 13. Comparison of the kinetic equation at different pH. (a) first-order kinetic model and (b) second order kinetic model. Temp = 25 °C; supersaturation = 2.04, seed loading = 100 mg; seed size 43.5 μm; agitation speed = 120 rpm.

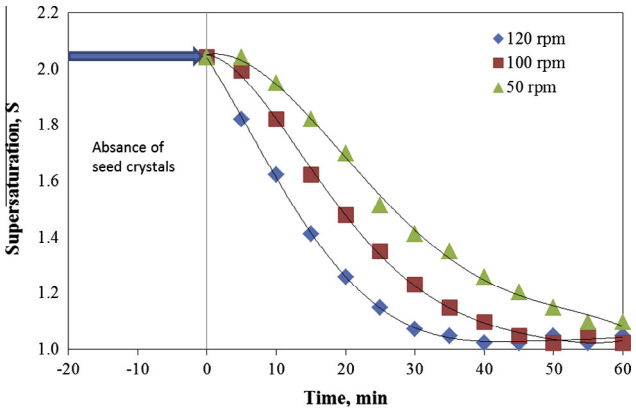

Fig. 15. Effect of stirrer speed on the decay of supersaturation. Solution pH = 9; supersaturation 2.04; Temp = 25 °C; seed loading = 100 mg; seed size = 43.5 μm.

model which also confirmed the high dependence of growth observed at higher stirrer speeds. Similar trend in the variation of the rate constant was observed by Nelson et al. [1] and Quintana et al. [44] for different experimental condition. The obtained first order rate constants (k_1) are 2.6, 3.7 and 5.8 h^{-1} at a speed of 50, 100, and 120 rpm, respectively. A significant increase in value of k is caused by higher turbulence level in the system resulted by agitation [45]. In addition, the higher agitation resulted in a thinner boundary layer as growth is mass transfer controlling.

3.5. Effect of temperature on struvite crystal kinetics

The effect of solution temperature on the decay of relative supersaturation of struvite was investigated in this study for a temperature range of 20–30 °C. Fig. 17 shows that the increasing temperature from 25 °C to 30 °C greatly enhances the growth rate of struvite formation. This study showed contradictory results conducted by Moussa et al. [23] where the decreasing growth rate of struvite was caused by different supersaturation used in temperatures range. Further, the decreasing growth rate was practically caused by low supersaturation at high temperature. The increasing growth rate may be caused by increasing activity of ions. At higher temperatures, the clusters adsorbed onto the crystal surface were more active in causing a higher surface-integration rate.

3.6. Diffusion–Reaction theory of struvite crystal growth mechanism: effect of various process parameters

There are also two major steps involved in the growth of a crystal [46] which are given below:

(i) convective transport of the solute from the bulk of the supersaturated solution to the surface of a crystal and;
(ii) surface integration or accumulation of the solute molecules in the growing layers of a crystal.

The crystal growth rate can be calculated based on the resistance offered by the above two steps. Second step followed first order kinetics and depends on the degree of supersaturation (C–C_S) at the crystal surface. Basically, crystals growth mechanism can be combined of diffusion and reaction processes and hence called diffusion–reaction theory of crystal growth [46,47]. The rate of increase in the mass of a single crystal can be written as:

$$\frac{dm_c}{dt} = K_L A_c (C - C_S) \tag{12}$$

where K_L is the overall mass transfer coefficient for the growth process which combines the above two resistance, m_c is mass of a single crystal, A_c is area of a single crystal, C is bulk solute concentration and C_s is saturation concentration of the solute at the given temperature.

Alternatively, growth rate can also be expressed as the rate of change of the "characteristic size" of a crystal. The characteristic size (L) is related to the mass (m_c), area (A_c) and volume (V_c) of a crystal through a "shape factor" as follows,

$$m_c = \rho_c \phi_c L^3; \quad A_c = \phi_a L^2 \text{ and } V_c = \phi_v L^3 \tag{13}$$

where ρ_c is crystal density (for struvite 1.7 g/cm^3), ϕ_v is volume shape factor (for cube 6) and ϕ_v is area shape factor (for cube 1).

Hence the crystal growth rate can also be expressed as

$$G = \frac{dL}{dt} = (K_L \phi_a / 3\rho_c \phi_v)(C - C_S) = K_G (C - C_S)/C_S = K_G (S - 1) \tag{14}$$

where G is a measure of the crystal growth rate and

$$K_G = K_L \phi_a C_S / 3\rho_c \phi_v \tag{15}$$

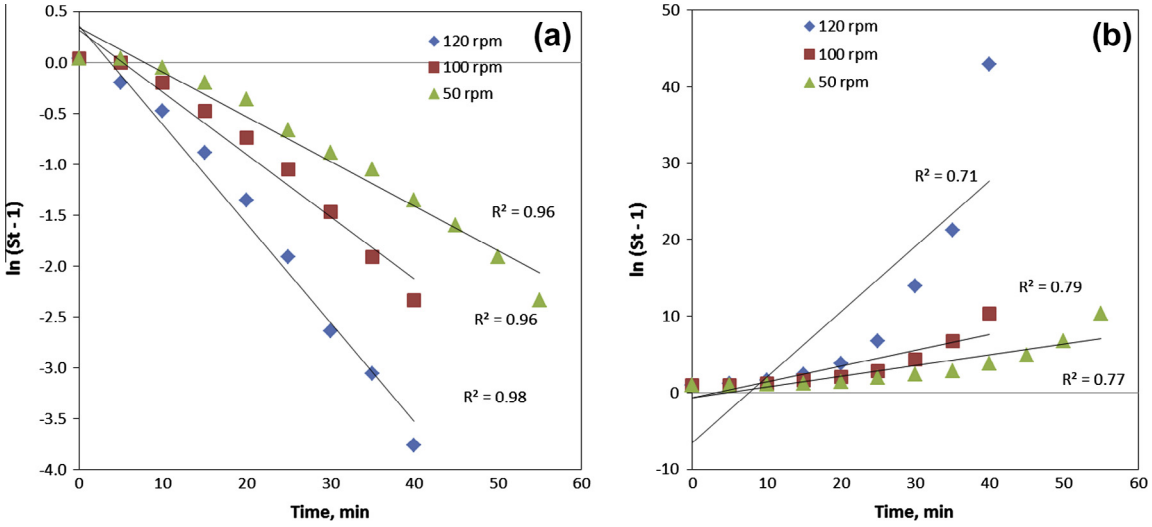

Fig. 16. Comparison of the kinetic equation at different stirrer speed between (a) first-order kinetic model and (b) second order kinetic model. Solution pH = 9; temp = 25 °C; supersaturation = 2.04; seed loading = 100 mg; seed size = 43.5 μm.

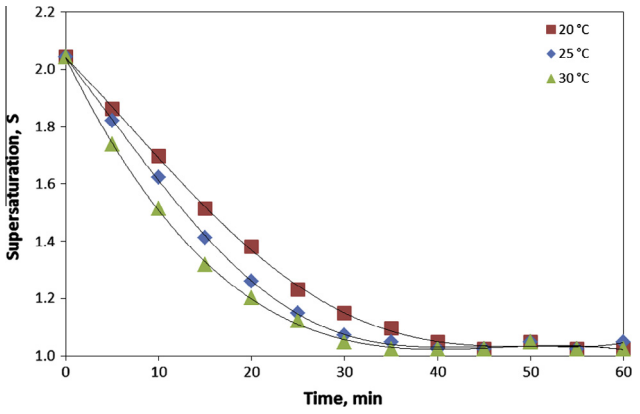

Fig. 17. Effect of temperature on decay of supersaturation of struvite precipitation. Solution pH = 9; supersaturation = 2.04, pH 9, 120 rpm; seed loading = 100 mg; seed size = 43.5 μm; agitation speed = 120 rpm.

Eq. (15) depends on the various system parameters such as supersaturation, solution pH, temperature and impurities NaCl addition. If the process is integration or accumulation of solute molecule on the surface of seed crystal, the above second step follows nonlinearity and hence the crystal growth can also be written as power law equation

$$G = \frac{dL}{dt} = K_G S^g \tag{16}$$

Or

$$\log G = \log K_G + g \log S \tag{17}$$

The above mechanistic power law growth rate equation was fitted with our batch struvite crystalliser experimental data. The overall mass transfer coefficient (K_L) can be obtained from the value of K_G at various physico-chemical process parameters. The slope of plot between log G versus log S gives the value of crystal growth order (g) parameter and intercepts give K_G value at different physico-chemical parameters.

Fig. 18 shows the effect of pH on crystal growth rate (G). Fig. 18 shows the growth rate mechanistic plot of Eq. (17) at different solution pH. Similarly all other growth kinetics fitted plots of Eq. (17) under crystal sizes, temperature, stirrer speed, NaCl addition which are not presented here. The fitted growth rate kinetic and mass transfer parameters under various physico-chemical parameters are presented in Table 2. From Table 2, higher linear

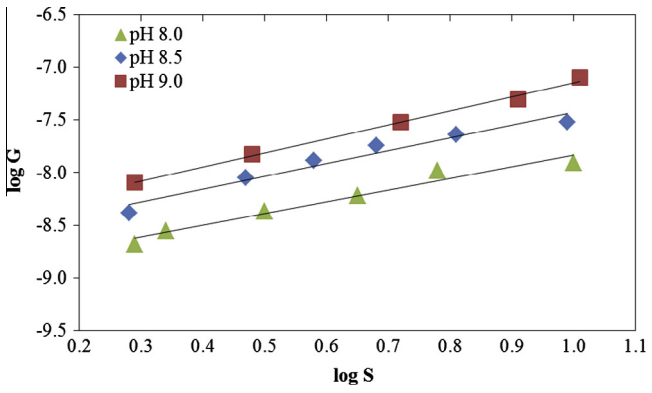

Fig. 18. Crystal growth rate of struvite as a function of supersaturation at various solution pH. Temp = 25 °C; supersaturation = 2.04; seed loading = 100 mg; seed size = 43.5 μm; agitation speed = 120 rpm.

regression coefficient (R^2) value indicates the applicability of power law diffusion–reaction mechanistic growth kinetic model. It can be observed that the growth rate increases with increase in supersaturation for all solution pH range. This is because of the increasing concentration driving forces.

Table 2 also showed the applicability of a first-order struvite growth kinetics (g = 1.1–1.3). According to Nielsen and Toft [48] the growth mechanism from surface integration (n = 2) to controlled diffusion (n = 1) was observed as the supersaturation of the solution increased, which was explained due to the increase of the mass transfer rate (K_L). In the present study, the growth kinetic order was indicated that the precipitation induced by struvite seed crystals is controlled by the diffusion step for all solution pH. The growth rate constants (K_G) were found to be function of solution pH (Table 2). The rate constant (K_G) value increases with increasing solution pH. The value of K_G under various process condition (Table 2) is very much comparative value reported by many other investigates for different struvite formation system [2,11,49,50]. The increase in the rate of crystal growth was attributable by increase in rate of desupersaturation. The increased decay of supersaturation rate would give more mass transfer (K_L) in which crystal growth could take place. Further, Table 2 also shows the overall mass transfer coefficient (K_L) which is calculated by Eq. (15) increased with increase in solution pH.

Table 2 presented various fitted growth kinetic and mass transfer parameters under various process conditions. The growth rate constant (K_G) increased with decrease in seed crystal. Increasing growth rate (K_G) of smallest crystal was caused by increasing mass-transfer of liquid to crystals. Table 2 shows that mass-transfer coefficient (K_L) increased with decrease in seed size.

The struvite growth rates were measured in the supersaturation range under the influenced of different temperatures of 20, 25 and 30 °C respectively. Therefore, Table 2 shows also that the growth rate constant (K_G) increased with increase in temperature. Based on the cluster transformation mechanism, activation of constituent ion in higher temperature may provide more available clusters for growth and it is possible that the transformation became more significant at higher temperature [51]. Thus, it can be indicated that the K_L values increased with increase in temperature (Table 2).

In order to estimate the activation energy of the growth of struvite, the activation energy of nucleation, E_{act}, has been calculated by the following Arrhenius equation;

$$K_G = K_0 \cdot \exp\left(\frac{-E_{act}}{RT}\right) \tag{18}$$

This empirical Eq. (18) may be simplified to:

$$\log K_G = \log K_0 - \frac{E_{act}}{2.303RT} \tag{19}$$

where K_0 is a constant, E_{act} is the activation energy (J mol^{-1}) for the process, and R is the gas constant (8.314 J/K mol). Activation energy represents the minimum energy that is required for a growth struvite crystal to take place. Fig. 19 is a plot of log K_G versus 1000/T for growth of struvite crystal obtained in temperature ranged examined, and the value of activation energy of growth of struvite crystals E_{act} of 55.42 kJ mol^{-1} were obtained from fitting experimental data.

Experiments were also conducted at different stirrer speed of 50, 100, and 120 rpm, at solution pH 9 and temperature of 25 °C in the crystalliser loaded with an appropriate amount struvite crystal seeds. The fitted growth model parameters are presented in Table 2 which indicates that the crystal growth rate increased with increase in stirrer speeds. The growth rate at different stirrer speed was also predicted by using power law expression of Eq. (17). The growth rate order changes between 1.2 and 1.3 with increased stir-

Table 2
Fitted struvite growth kinetic and mass transfer parameters under various process condition.

Process variable	Mean saturation concentration (C_S), mMol/L	Growth Parameters			Overall mass transfer coefficient
		g	$K_G \times 10^{-9}$, m/s	R^2	$K_L \times 10^{-5}$, m/s
Solution pH					
8.0	1.9	1.12	1.1	0.96	0.20
8.5	1.2	1.22	2.3	0.95	0.66
9.0	0.8	1.36	3.3	0.97	1.43
Crystal size (μm)					
24.3	0.8	1.41	4.1	0.98	1.78
43.5	0.8	1.22	2.3	0.95	1.00
84.8	0.8	1.08	1.2	0.97	0.52
Temperature (°C)					
20	0.7	1.05	2.5	0.98	1.24
25	0.8	1.36	3.3	0.97	1.43
30	0.9	1.47	5.2	0.98	2.00
Stirrer speed (rpm)					
50	0.8	1.21	0.5	0.98	0.22
100	0.8	1.26	1.6	0.97	0.69
120	0.8	1.36	3.3	0.98	1.43
NaCl addition (ppm)					
0	0.8	1.22	3.3	0.97	1.43
50	0.8	1.27	4.8	0.96	2.08
100	0.8	1.33	9.0	0.98	3.90
200	0.8	1.38	10.0	0.97	4.33

rer speed in struvite system (Table 2). These values indicate that the crystal growth of struvite is controlled by a combination of controlled diffusion step I and surface integration of step II. Moreover, the constant value of K_G and K_L increased with higher stirrer speed. It is evident that growth rate of struvite crystal increased with stirrer speed. However, an increasing stirrer speed is not always advantageous in an operation, since the increasing stirrer speeds may cause crystal breakage. This is because of collisions among crystals, collision of crystal with crystalliser wall, baffle and impeller surface, etc. On the other hand, at lower stirrer speed not much crystals mass were visible in suspension zone. Higher supersaturation is favourable for the faster growth of the small crystals. When the small crystals grow to large crystals, the large crystals have higher settling velocities and need larger stirrer speed to be stay in solution. As a result, of the relative speed between the crystals and the solution will increase the crystal size and leads to a faster mass transfer step in, i.e. faster growth rate [3].

The presence of impurities or foreign ions in a system may enhance or suppress the growth. In this present study, NaCl was used as impurity in struvite system. Experiments were conducted for various NaCl concentrations of 50, 100, and 200 ppm in aqueous solution of struvite. The crystal growth rates were evaluated by decay of relative supersaturation of solution at various NaCl concentrations and also without NaCl addition. Fig. 20 shows that

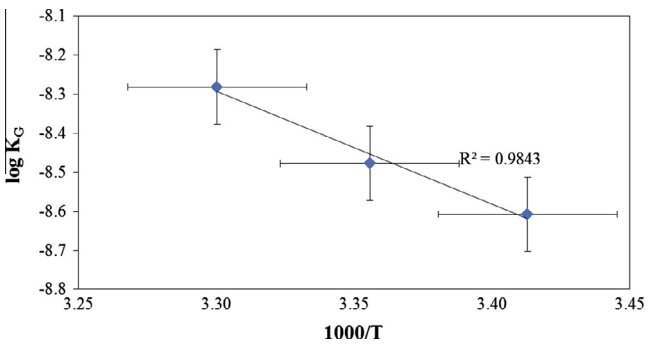

Fig. 19. An Arrhenius plot Eq. (19) for struvite crystal with 5% error bar.

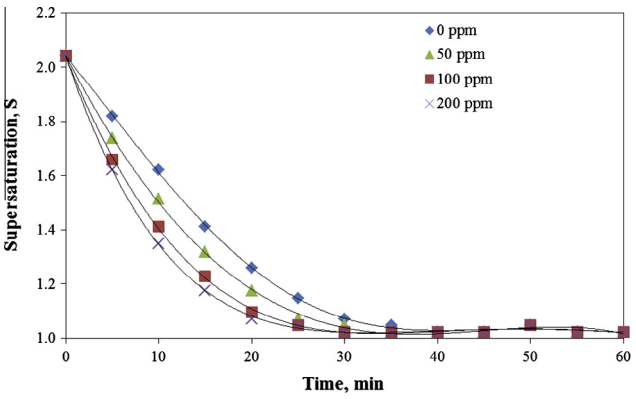

Fig. 20. Effect of NaCl on decay of supersaturation of struvite precipitation. Solution pH = 9; Temp = 25 °C; supersaturation 2.04; seed loading = 100 mg; seed size = 43.5 μm; agitation speed = 120 rpm.

the crystal growth rate of struvite increases with increasing NaCl concentration. The linearised struvite growth kinetics plots based on power law expression of Eq. (17) are not presented here. However, growth kinetic fitting parameters at different NaCl concentration are presented in Table 2. It was found from Table 2 that NaCl addition in a system can have a significant effect on the growth of struvite crystals. Higher growth rate (K_G) at higher NaCl concentration was obtained. In this situation, the NaCl addition may not only change the properties of solution but also alter the characteristic of the adsorption layer at the crystal-solution interface [52]. According to Tai et al. [42], the increased presence of NaCl in the system decreased the double-layer thickness between solution and crystal, so the adsorption of growth unit takes place due to lower resistance offered by thinner boundary layer thickness.

Further from Table 2 the growth rate order (g) was between 1.22 and 1.38. Moreover, NaCl concentration-dependent growth rate of struvite plot is shown in Fig. 21. The growth rate constant K_G tends to be constant for high concentration of NaCl. Thus from Fig. 21, the crystal growth process of struvite is diffusion controlled for NaCl addition below 100 ppm. As NaCl addition increases, the

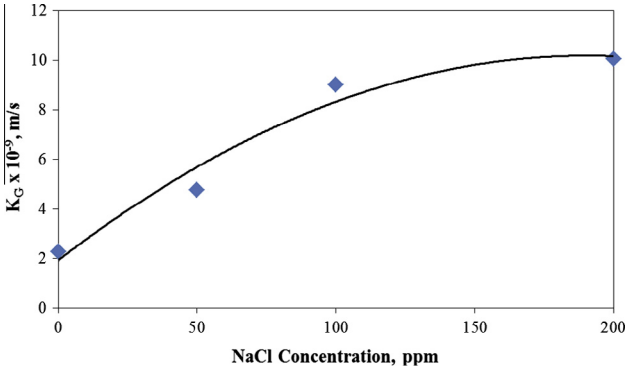

Fig. 21. Plots of growth rate constant (K_G) versus NaCl concentration addition.

mass transfer becomes significant (K_L). After the NaCl addition exceeds 100 ppm, the coefficients are constant, giving a constant growth rate.

4. Conclusions

Struvite ($MgNH_4PO_4{\cdot}6H_2O$) is the mineral phase obtained in wastewater treatment and purification plants besides being an important common component of urinary tract calculi. The impacts of physico-chemical process parameters such as seed loading, temperature, solution pH, stirrer speed, and impurities on struvite crystal growth mechanism have been successfully investigated. The kinetic rate of decay of supersaturation was identified by using supersaturation 2.04 which is close to the solubility curve. Effect of seed loading may increase rate of struvite precipitation. The pseudo-first order and pseudo-second order kinetic models are employed to analyse the rate of decay of supersaturation at different process conditions. The experimental results fitted well with the first-order growth kinetic model. The obtained first-order rate constant, k, can be used to explain the struvite precipitation behaviour. In the batch stirrer crystalliser, struvite precipitation was strongly dependent of solution pH, temperature and stirrer speed.

A classical diffusion–reaction mass transfer crystal growth mechanism is applicable under various physico-chemical process parameters to identify the growth mechanism. The various growth kinetic parameters and overall mass transfer coefficients under various process conditions have been determined. These crystal kinetic growth informations are essential for the design and optimisation of struvite crystalliser and thus control of struvite formation. It has also application of struvite precipitation recycling technology. Struvite crystallisation could be an alternative for the sustainable and economical recovery of phosphorous from concentrated wastewater stream.

References

[1] K.S.L. Corre, E. Valsami-Jones, P. Hobbs, S.A. Parsons, Impact of calcium on struvite crystal size, shape and purity, Journal of Crystal Growth 283 (2005) 514–522.
[2] A. Matynia, J. Koralewska, B. Wierzbowska, K. Piotrowski, The influence of process parameters on struvite continuous crystallization kinetics, Chemical Engineering Communications 193 (2006) 160–176.
[3] M.I.H. Bhuiyan, D.S. Mavinic, R.D. Beckie, Nucleation and growth kinetic of struvite in a fluidized bed reactor, Journal of Crystal Growth 310 (2008) 1187–1194.
[4] K.N. Ohlinger, T.M. Young, E.D. Schroeder, Kinetics effects on preferential struvite accumulation in wasterwater, Journal of Environmental Engineering 125 (1999) 730–737.
[5] K.S.L. Corre, E. Valsami-Jones, P. Hobbs, B. Jefferson, S.A. Parsons, Agglomeration of struvite crystals, Water Research 41 (2007) 419–425.
[6] G. Kurtulus, A.C. Tas, Transformations of neat and heated struvite ($MgNH_4PO_4{\cdot}6H_2O$), Materials Letters 65 (2011) 2883–2886.
[7] A.G. Jones, Crystallization process system, first ed., Butterworth-Heinemann, Oxford, 2002.
[8] A.S. Myerson, Handbook of industrial crystallization, second ed., Butterworth-Heinemann, Woburn (USA), 2002.
[9] O. Söhnel, J. Garside, Precipitation: basic principles and industrial applications, First ed., Butterworth-Heinemann, Oxford, 1992.
[10] A. Mersmann, Crystallization Technology Handbook, second ed., Marcel Dekker Inc., New York, 2001.
[11] C.M. Mehta, D.J. Batstone, Nucleation and growth kinetics of struvite crystallization, Water Research 47 (2013) 2890–2900.
[12] E. Ariyanto, H.M. Ang, T.K. Sen, Impact of various physico-chemical parameters on spontaneous nucleation of struvite ($MgNH_4PO_4{\cdot}6H_2O$) formation in a wastewater treatment plant: kinetic and nucleation mechanism, Desalination and Water Treatment (2013) 1–12 (10(1080/19443994), 2013, 821042).
[13] W. Stumm, J.J. Morgan, Aquatic Chemistry: An Introduction Emphasizing Chemical Equilibria in Natural Waters, John Wiley and Sons Ltd., Canada, 1981.
[14] P. Battistoni, A.D. Angelis, P. Pavan, M. Prisciandaro, F. Cecchi, Phosphorus removal from a real anaerobic supernatant by struvite crystallization, Water Research 35 (2001) 2167–2178.
[15] I. Celen, M. Türker, Recovery of ammonia as struvite from anaerobic digester effluents, Environmental Technology 22 (2001) 1263–1272.
[16] E.V. Münch, K. Barr, Controlled struvite crystallisation for removing phosphorus from anaerobic digester sidestreams, Water Research 35 (2001) 151–159.
[17] I. Stratful, M.D. Scrimshaw, J.N. Lester, Conditions influencing the precipitation of magnesium ammonium phosphate, Water Research 35 (2001) 4191–4199.
[18] N.O. Nelson, R.L. Mikkelsen, D.L. Hesterberg, Struvite precipitation in anaerobic swine lagoon liquid: effect of pH and Mg:P ratio and determination of rate constant, Bioresource Technology 89 (2003) 229–236.
[19] A.E. Durrant, M.D. Scrimshaw, I. Stratful, J.N. Lester, Review of the feasibility of recovering phosphate from wastewater for use as a raw material by the phosphate industry, Environmental Technology 20 (1999) 749–758.
[20] H.K. Aage, B.L. Andersen, A. Blom, I. Jensen, The solubility of struvite, Journal of Radio Analytical and Nuclear Chemistry 223 (1997) 213–215.
[21] J.R. Burns, B. Finlayson, Solubility product of magnesium ammonium phosphate hexahydrate at various temperatures, The Journal of Urology 128 (1982) 426–428.
[22] M.I.H. Bhuiyan, D.S. Mavinic, R.D. Beckie, A solubility and thermodynamic study of struvite, Environmental Technology 28 (2007) 1015–1026.
[23] S.B. Moussa, M.M. Tlili, N. Batis, M.B. Amor, Influence of tempereature on struvite precipitation by CO_2-deagassing method, Crystal Research and Technology 46 (2011) 255–260.
[24] S. Uludag-Demirer, M. Othman, Removal of ammonium and phosphate from the supernatant of anaerobically digested waste activated sludge by chemical precipitation, Bioresource Technology 100 (2009) 3236–3244.
[25] D. Kim, J. Kim, H.D. Ryu, S.I. Lee, Effect of mixing on spontaneous struvite precipitation from semiconductor wastewater, Bioresource Technology 100 (2009) 74–78.
[26] A. Triger, J.S. Pic, C. Cabassud, Determination of struvite crystallization mechanisms in urine using turbidity measurement, Water Research 46 (2012) 6084–6094.
[27] I. Kabdasli, S.A. Parsons, O. Tünaya, Effect of major ions on induction time of struvite precipitation, Croatica Chemica Acta 79 (2006) 243–251.
[28] D.L. Parkhurst, C.A.J. Appelo, User's Guide To Phreeqc (Version 2) – A Computer Program For Speciation, Batch-Reaction, One-Dimensional Transport, And Inverse Geochemical Calculations, Denver, Colorado, 1999.
[29] M. Quintana, E. Sanchez, M.F. Colmenarejo, J. Barrera, G. Garcia, R. Borja, Kinetics of phosphorus removal and struvite formation by the utilization of by-product of magnesium oxide production, Chemical Engineering Journal 111 (2005) 45–52.
[30] M.S. Rahaman, N. Ellis, D.S. Mavinic, Effects of various process parameters on struvite precipitation kinetics and subsequent determination of rate constants, Water Science and Technology 57 (2008).
[31] C.K. Chauhan, K.C. Joseph, B.B. Parekh, M.J. Joshi, Growth and characterization of struvite crystals, Indian Journal of Pure and Applied Physics 46 (2008) 507–512.
[32] E. Banks, R. Chianelli, R. Korenstein, Crystal chemistry of struvite analogs of the type $MgMPO_4{\cdot}6H_2O$ (M+ = potassium(1+), rubidium(1+), cesium (1+), thallium(1+), ammonium(1+), Inorganic Chemistry 14 (1975) 1634–1639.
[33] K. Suguna, M. Thenmozhi, C. Sekar, Growth, spectral, structural and mechanical properties of struvite crystal grown in presence of sodium fluoride, Bulletin of Materials Science 35 (2012) 701–706.
[34] E. Ariyanto, Crystallisation and dissolution studies of struvite in aqueous solution, in: Chemical Engineering, Curtin University, Perth, 2013.
[35] N.C. Bouropoulos, P.G. Koutsoukos, Spontaneous precipitation of struvite from aqueous solutions, Journal of Crystal Growth 213 (2000) 381–388.
[36] M.I.H. Bhuiyan, D.S. Mavinic, F.A. Koch, Thermal decomposition of struvite and its phase transition, Chemosphere 70 (2008) 1347–1356.
[37] P.J. Frawley, N.A. Mitchell, C.T. O'Ciardha, K.W. Hutton, The effects of supersaturation, temperature, agitation and seed surface area on the secondary nucleation of paracetamol in ethanol solutions, Chemical Engineering Science 75 (2012) 183–197.
[38] D.C. Huang, W. Liu, S.K. Zhao, Y.Q. Shi, Z.X. Wang, Y.M. Sun, Quantitative design of seed load for solution cooling crystallization based on kinetic analysis, Chemical Engineering Journal 156 (2010) 360–365.

[39] P.W.A. Perera, W.X. Wu, Y.X. Chen, Z.Y. Han, Struvite recovery from swine waste biogas digester effluent through a stainless steel device under constant pH conditions, Biomedical and Environemental Sciences 22 (2009) 201–209.
[40] W. Omar, J. Ulrich, Influence of crystallization conditions on the mechanism and rate of crystal growth of potassium sulphate, Crystal Research and Technology 34 (2003) 34–41.
[41] A. Adnan, M. Dastur, D.S. Mavinic, F.A. Koch, Preliminary investigation into factors affecting controlled struvite crystallization at the bench scale, Journal of Environmental Engineering and Science 3 (2004) 195–202.
[42] C.Y. Tai, P.C. Chen, T.M. Tsao, Growth kinetics of CaF_2 in a pH-stat fluidized-bed crystallizer, Journal of Crystal Growth 290 (2006) 576–584.
[43] N. Stubičar, B. Marković, A. Tonejc, M. Stubičar, Crystal growth of lead fluoride phases using the constant composition method III. Effect of pH and ionic strength, Journal of Crystal Growth 130 (1993) 300–304.
[44] L. Pastor, D. Mangin, R. Barat, A. Seco, A pilot-scale study of struvite precipitation in a stirred tank reactor: conditions influencing the process, Bioresource Technology 99 (2008) 6285–6691.
[45] S. Uludag-Demirer, G.N. Demirer, S. Chen, Ammonia removal from anaerobically digested dairy manure by struvite precipitation, Process Biochemistry 40 (2005) 3667–3674.
[46] B.K. Dutta, Principles of Mass Transfer And Separation Processes, PHI Learning Pvt. Ltd., New Delhi, 2007.
[47] W.L. McCabe, J. Smith, P. Harriott, Unit Operations of Chemical Engineering, McGraw-Hill, Education, 2005.
[48] A.E. Nielsen, J.M. Toft, Electrolyte crystal growth kinetics, Journal of Crystal Growth 67 (1984) 278–288.
[49] J. Koralewska, K. Piotrowski, B. Wierzbowska, A. Matynia, Nucleation and crystal growth rates of struvite in DTM type crystallizer with a jet-pump of descending suspension flow in a mixing chamber, American Journal of Agricultural and Biological Sciences 2 (2007) 260–266.
[50] N. Hutnik, A. Kozik, A. Mazienczuk, K. Piotrowski, B. Wierzbowska, A. Matynia, Phosphates (V) recovery from phosphorus mineral fertilizers industry wastewater by continuous struvite reaction crystallization process, Water Research 47 (2013) 3635–3643.
[51] M.C. Chang, C.Y. Tai, Effect of the magnetic field on the growth rate of aragonite and the precipitation of $CaCO_3$, Chemical Engineering Journal 164 (2010) 1–9.
[52] J.W. Mullin, Crystallization, fourth ed., Butterworth-Heinemann, Oxford, 2001.